Optics Letters

Manipulation of the spontaneous parametric down-conversion process in space and frequency domains via wavefront shaping

YAJUN PENG,[1,2] YANQI QIAO,[1,2] TONG XIANG,[1,2] AND XIANFENG CHEN[1,2,*]

[1]State Key Laboratory of Advanced Optical Communication Systems and Networks, School of Physics and Astronomy, Shanghai Jiao Tong University, Shanghai 200240, China
[2]Key Laboratory for Laser Plasma (Ministry of Education), Collaborative Innovation Center of IFSA (CICIFSA), Shanghai Jiao Tong University, Shanghai 200240, China
*Corresponding author: xfchen@sjtu.edu.cn

Received 22 June 2018; accepted 15 July 2018; posted 23 July 2018 (Doc. ID 335891); published 14 August 2018

The spontaneous parametric down-conversion (SPDC) source of entangled-photon pairs is important for applications in the quantum information process and quantum communication, but suffers from scattering by sample defect and air impurity. Here, we proposed an alternative scheme to manipulate the scattered SPDC process, where only a spatial light modulator was used to control the incident wavefront. The scheme was experimentally tested and also applied on the manipulation of photon pairs through the SPDC process with spectral control. This work proved the feasibility of manipulating nonlinear signals at quantum level with feedback-based wavefront shaping and also indicated applications in long-distance quantum key distribution, quantum communications, and quantum imaging, especially in complex environments.

OCIS codes: (270.5565) Quantum communications; (190.4410) Nonlinear optics, parametric processes; (140.3300) Laser beam shaping; (070.6120) Spatial light modulators.

https://doi.org/10.1364/OL.43.003985

Entanglement is the main resource for many applications of quantum information processing, including quantum key distribution (QKD) [1–3], quantum teleportation [4,5], and quantum imaging [6]. The standard source of entangled-photon pairs is nowadays the nonlinear optical process of spontaneous parametric down-conversion (SPDC) in optics. SPDC sources of entangled-photon pairs of high quality and brightness can be routinely realized using various methods in nonlinear bulk crystal, waveguide crystal, and optical fiber [7–11]. In reality, photon pair generation and propagation with long distance in free space will be scattered by sample defect and air impurity, which influences the efficiency of propagation and even the rate of reception [12]. Hence, an appropriate way to restore the SPDC process is desired.

Feedback-based wavefront shaping (FBWS) was experimentally proved a new and valid method of optical focusing and imaging through complex scattering media in 2007 [13], where the incident light is scattered to form a random speckle pattern and then recovered by using an optimization algorithm to control the phase of incident light [14–16]. In recent decades, wavefront shaping has been widely used in linear and nonlinear optics [17–19]. With the rapid development of adaptive optics, the application of FBWS has been extended to various fields, such as biomedical optics [16] and quantum optics [20,21].

Here, we demonstrated an adaptive scheme for manipulating the SPDC process with spectral control via FBWS through scattering media. In the experiment, we first modulated pump phase based on FBWS to compensate the domain structure's scattering effect of periodically poled lithium niobate (PPLN) to restore the SPDC process. The heralding efficiency was improved by 26.6%. Second, while propagating through long distance in free space, photon pairs would encounter the impurity in the air. The scattering media were added to simulate the impurity. The heralding efficiency was recovered to 94.6% of the value obtained in the experiment without scattering media. Third, the manipulation of the SPDC process with spectral control was also realized. Arbitrary wavelengths in the broadband emission could be selected to enhance by around 96%. Our scheme provides an alternative way for manipulating SPDC photon pairs in both space and frequency domains. It not only further proved the application of FBWS in nonlinear optics, but also showed the possibility for controlling quantum signals.

The schematic configuration is shown in Fig. 1. Without wavefront shaping, photon pairs were both generated and scattered from PPLN because of the domain structure's defect [22,23], then further scattered by air impurity when propagating with long distance in free space [Fig. 1(a)]. A spatial light modulator (SLM) was applied to modulate pump phase, which compensated the scattering effect and increased the signal intensity [Fig. 1(b)]. The concept of the SPDC process with spectral control via FBWS could be described by a simple model theoretically. As the signal and idler photons were scattered,

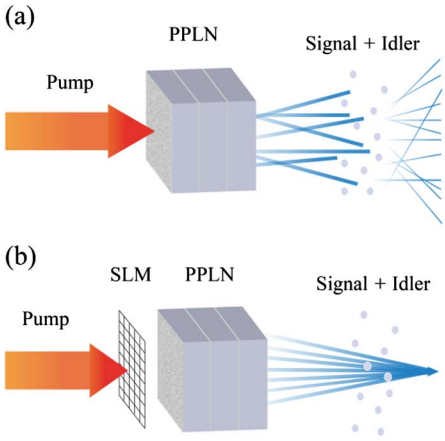

Fig. 1. Schematic configuration of the experiment. (a) Without wave-front shaping, signal and idler photons were generated from PPLN and scattered by structure defects of PPLN and air impurity. (b) SPDC focus with appropriate phase of pump by using SLM.

they formed a speckle pattern with a broadband spectrum. The broadband characterization of the signals and idlers through scattering media was described by the multispectral transmission matrix [24,25]. The overall output photons at the detected target at the wavelength of λ_k show

$$|n^{\text{out}}(\lambda_k)\rangle = \sum_{i=1}^{N} \alpha_{ik} e^{i\varphi_{ik}} |n_i^{\text{in}}(\lambda_k)\rangle, \tag{1}$$

where $\alpha_{ik}e^{i\varphi_{ik}}$ is the coefficient of the multispectral transmission matrix with φ_{ik} being the spectral phase component and, $|n_i^{\text{in}}(\lambda_k)\rangle$ is the input photon. The summation represents the integration of all SLM segments. The spectrum is given by the defined integral of overall wavelengths. φ_{ik} can be optimized by FBWS, which lead to a coherent superposition of selected wavelength λ_k.

Pairs of single photons in our experiment were generated under the setup as shown in Fig. 2(a). The pump light source was a pulse laser with the center wavelength at 1556 nm,

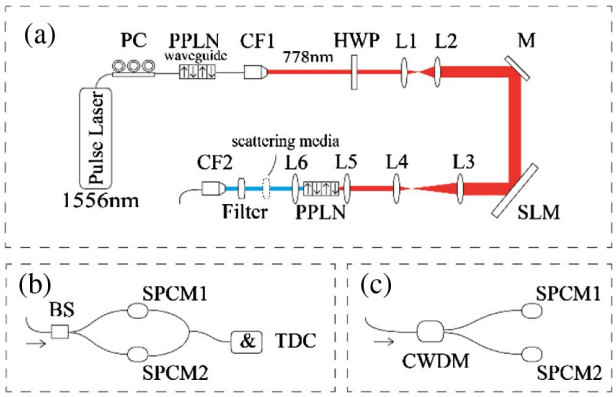

Fig. 2. Schematic of experimental setup. EDFA, erbium-doped fiber amplifier; PC, polarization controller; HWP, half-wave plate; M, mirror; Lens, L_{1-6} (f_{1-5} = 30 mm, 500 mm, 200 mm, 50 mm, 10 mm, 10 mm); SLM, spatial light modulator; CF1, 2, collimator fiber; BS, fiber beam splitter; SPCM 1, 2, single-photon counting module; TDC, time-to-digital converter.

a pulse width of 1.0 ns, and repetition rate of 10 MHz. It was amplified by an erbium-doped fiber amplifier and converted via second-harmonic generation (SHG) in a PPLN waveguide. A polarization controller was used to ensure the high efficiency of SHG. The emitted laser centered at 778 nm was then used to pump the PPLN bulk to generate photon pairs. Here, two collimator fibers (CF1 and CF2) with high transmission at 780 nm and 1560 nm, respectively, were applied. A half-wave plate was used after the pump for polarization control because of the response characteristics of the SLM. Lens 1 and lens 2 were used as the expanding system in order to pump more SLM area, which was composed of 192 × 1080 pixels, each with a rectangular area of 8 μm × 8 μm. The SLM, lens 3, lens 4, and lens 5 formed a $4f$-optical imaging system. In our experiment, the nonlinear crystal to generate collinear photon pairs is a type-0 PPLN bulk, 1 cm in length. A filter was then used to reject the pump laser.

The detector setups for scattering compensation and SPDC spectral control are shown in Figs. 2(b) and 2(c), respectively. The SPDC photons were separated by a 50:50 single-mode fiber beam splitter (BS) or filtered by different channels of the coarse wavelength division multiplexing (CWDM). The single-photon counting module (SPCM) (10 ± 0.2% quantum efficiencies and about 100 dark counts) was applied to count photon pairs. SPCM1 was extern-triggered by SPCM2, in order to obtain the heralding efficiency (H) by measuring the conditional detection efficiency (η_D) of heralded photons [26,27]. η_D was defined as the coincidence counting rate (R_C) divided by the trigger photon detection rate (R), such that

$$\eta_D = R_C/R. \tag{2}$$

H was corrected by considering transmittances of all optical elements (η) shown as

$$H = \eta_D/\eta, \tag{3}$$

where η included SPCM1 and 2 quantum efficiencies of 10%, the influence of BS, estimated 4% reflection loss upon CF1 into free space, 5% loss due to the antireflection-coated surfaces of the five lenses, and the filter transmission of 95% at 1560 nm. Then two output ports of SPCM 1 and 2 were both connected to a time-to-digital converter (TDC) to measure the coincidence count in Fig. 2(b). All SLM and SPCMs were connected to a computer with a genetic algorithm (GA) for optimization. Here, H served as the feedback signal, and GA was selected in the optimization process because it worked better in noisy environments [26]. All SLM pixels were regrouped and subdivided into 32 × 18 phase segments (N) for a faster optimization speed.

The temperature of PPLN was adjusted at 320 ± 0.1 K in order to meet the quasi-phase matching (QPM) condition. The CF2 was adjusted to get the maximum SPCM count. First of all, scattering media were not added, and the detector setup in Fig. 2(b) was applied. A typical compensation result of the domain structure's scattering effect is shown in Fig. 3. The heralding efficiency H increased with the iteration as expected and eventually reached a stable value. After 30 iterations, maximum H arrived at 41.9% [Fig. 3(a)]. In other words, when a signal photon is detected by an SPCM, the probability of its twin idler photon being present is 41.9% [27]. H was improved by 26.6% because the structure defect of PPLN was partly compensated by the optimization process. The final H was

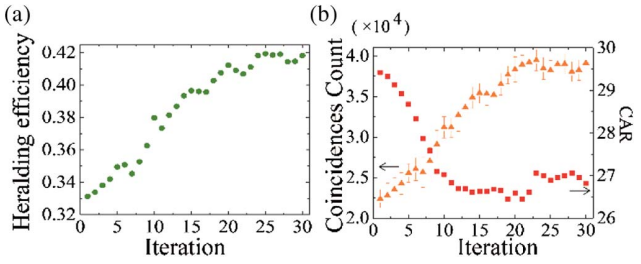

Fig. 3. (a) Heralding efficiency of the SPCM count for each generation. A typical value was estimated to be 41.9% after 30 iterations. (b) Yellow triangles and red squares represent the coincidence events and the ratio of coincidences to accidentals, respectively.

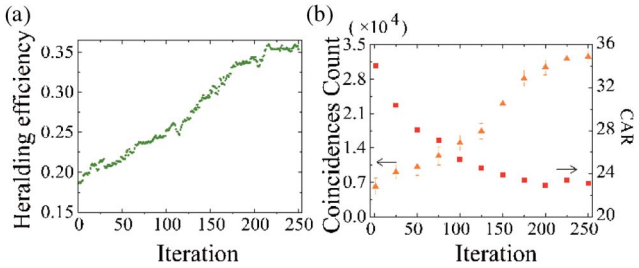

Fig. 4. (a) Heralding efficiency of the SPCM count for each generation. A typical value was estimated to be 36.0% after 250 iterations. (b) Yellow triangles and red squares represent the coincidence events and the ratio of coincidences to accidentals, respectively.

determined by the scattering strength of the PPLN domain structure and the number of defects in the crystal itself. It also depended on some details of GA, such as the segment size and mutation probability [28]. There are also many other optimization algorithms valid for the procedure, such as the continuous sequential algorithm, transmission matrix, and ant colony optimization. Each optimization algorithm has its exclusive characteristics but may not be well suited for noisy environments [28–30]. GA has its particular advantages in low signal-to-noise environment, and the convergence is fast, so it was chosen to do the optimization.

In traditional quantum researches, the coincidence count and the ratio of coincidences to accidental (CAR) were usually used to describe the entangled-photon pairs quality. Coincidences per pulse generated through SPCD can be expressed as

$$C = \mu\eta_s\eta_i, \tag{4}$$

where μ is the number of pairs generated per pulse, η_s and η_i are the overall collection efficiencies for the signal and idler photons, respectively [31]. CAR was calculated by taking the ratio of coincidences to accidentals such that

$$\mathrm{CAR} = C/[(\mu\eta_s + d_s)(\mu\eta_i + d_i)], \tag{5}$$

where d_s and d_i are the dark counts in the signal and idler detectors, respectively. In our experiment, d_s compared to $\mu\eta_s$ or d_i compared to $\mu\eta_i$ is small enough. So, we can substitute C in the denominator to obtain an equation that is dependent only on μ, which is

$$\mathrm{CAR} = 1/\mu. \tag{6}$$

In our experimental setup, the coincidence events were averaged five times every 60 s during each iteration. As shown in Fig. 3(b), the coincidence count (C) increased, and the CAR decreased (μ increased) with the iteration increasing, which proved the entangled-photon pairs were indeed increasing under the optimization. At the same time, the multiphoton effect was stronger because μ increased, which showed the noisy environments. In Eq. (2), η_s and η_i were regarded as equal in estimation, which includes the collection efficiency and quantum efficiencies of SPCM in our experiment. The heralding efficiency H is identical to the collection efficiency. The increase of H and the decrease of CAR demonstrated that the FBWS optimization not only compensated for the scattering due to defects in PPLN but also increased collection efficiency.

Second, a scattering medium was added behind PPLN to simulate the air impurity that photon pairs propagating with long distance in free space would encounter [Fig. 2(a)]. In our experimental design, the scattering medium was some TiO_2 nanoparticles deposited on an indium-tin oxide coated glass substrate by an electrophoresis method [32]. The detector setup is shown in Fig. 2(b). The initial value of H was 38.7%, and it was down by 50.9% after adding the scattering medium. During a similar optimization, it was increasing with the iteration as expected, and the saturated value was 36.0% after 250 iterations [Fig. 4(a)]. That means the scattering effect by the turbid medium has been compensated by 94.6%. During optimization, the coincidence events and CAR of each generation were also measured and are presented in Fig. 4(b), showing a conclusion similar to the above. The optimization needs more time (iterations) to achieve saturation. H was lower but improved by 92.7% because of the stronger scattering effect. Generally speaking, our scheme is more efficient, especially for an extra scattering medium or samples with defects. What is more, focusing and quantum imaging could be expected with an electron multiplying charge-coupled device or other quantum detectors.

Furthermore, manipulation of the SPDC process with spectral control was realized, indicating possible applications of long-distance quantum communication in complex environments. The experimental setup is illustrated in Figs. 2(a) and 2(c). The SPDC photons with 70 nm bandwidth (from 1530 nm to 1600 nm [33]) were divided by the CWDM with 13 nm bandwidth in each channel. As the theory in Eq. (1), any channel could be chosen to be enhanced by FBWS. For example, signals and idlers in different channels with central wavelengths of 1550 nm and 1570 nm were detected by SPCM1 and SPCM2, respectively. SPCM1 was extern-triggered by SPCM2, in order to obtain H. Then H of frequency-conjugate pairs was regarded as the feedback for optimization. The initial value of H was about 18.2%. After optimization, H was estimated to be 37.2%. Besides the feedback wavelength, the H of another frequency-conjugate pair (1530 nm and 1590 nm) was measured before and after optimization. During this similar optimization, we regarded H (frequency-conjugate pairs from 1530 nm and 1590 nm channels) as the feedback and repeated the experiment. Some typical results are shown in Table 1.

There was also a little enhancement of the nearby wavelengths in the optimization, similar to some previous results because of the total signal enhancement [25]. With the improvement of the detection efficiency and algorithms, dense

Table 1. Value of *H* Before and After Optimization for 1550 nm and 1590 nm, Respectively[a]

ω (nm)	1530/1590	1550/1570	1550/1570	1530/1590
Before	17.8%	**18.2%**	17.6%	**18.0%**
After	32.2%	**37.2%**	30.5%	**35.4%**

[a]ω is the central wavelength of the CWDM.

wavelength division multiplexing was expected in our experimental setup to realize spectral control of SPDC photons with narrower bandwidth. The same experimental setup can also be applied to other linear optics or nonlinear frequency conversion in quantum level.

In conclusion, we put forward a method of manipulating the SPDC process in space and frequency domains theoretically and experimentally. First, the pump phase was modulated to compensate the structure scattering effect of PPLN, which enhanced the SPDC process by *H* 41.9%. Second, a scattering medium was used to simulate the air impurity that SPDC photon pairs propagating in long distance may suffer, and this scattering effect was compensated by 94.6%. Finally, manipulation of the SPDC process with spectral control was realized. This work proved the possibility of manipulating nonlinear signals at quantum level with FBWS and also indicated applications in long-distance QKD, quantum communications, and quantum imaging, especially in complex environments.

Funding. National Key R&D Program of China (2017YFA0303700); National Natural Science Foundation of China (NSFC) (11734011); Foundation for Development of Science and Technology of Shanghai (17JC1400400).

REFERENCES

1. C. Z. Peng, J. Zhang, D. Yang, W. B. Gao, H. X. Ma, H. Yin, H. P. Zeng, T. Yang, X. B. Wang, and J. W. Pan, Phys. Rev. Lett. **98**, 010505 (2007).
2. J. L. Smirr, S. Guilbaud, J. Ghalbouni, R. Frey, E. Diamanti, R. Alleaume, and I. Zaquine, Opt. Express **19**, 616 (2010).
3. C. Erven, D. Hamel, K. Resch, R. Laflamme, and G. Weihs, in *International Conference on Quantum Comunication and Quantum Networking* (2009), Vol. **36**, p. 108.
4. D. Bouwmeester, J. Pan, K. Mattle, M. Eibl, H. Weinfurter, and A. Zeilinger, Nature **390**, 575 (1997).
5. Y. Kim, S. Kulik, and Y. Shih, Phys. Rev. Lett. **86**, 1370 (2001).
6. G. Brida, M. Genovese, and I. R. Berchera, Nat. Photonics **4**, 227 (2010).
7. P. Kwiat, E. Waks, A. White, I. Appelbaum, and P. Eberhard, Phys. Rev. A **60**, R773 (1999).
8. A. Martin, A. Issautier, H. Herrmann, W. Sohler, D. Ostrowsky, O. Alibart, and S. Tanzilli, New J. Phys. **12**, 103005 (2010).
9. E. Pomarico, B. Sanguinetti, N. Gisin, R. Thew, H. Zbinden, G. Schreiber, A. Thomas, and W. Sohler, New J. Phys. **11**, 113042 (2009).
10. K. Lee, J. Chen, C. Liang, X. Li, P. Voss, and P. Kumar, Opt. Lett. **31**, 1905 (2006).
11. X. Li, P. Voss, J. Sharping, and P. Kumar, Phys. Rev. Lett. **94**, 053601 (2005).
12. S. Liao, W. Cai, W. Liu, L. Zhang, Y. Li, J. Ren, J. Yin, Q. Shen, Y. Cao, Z. Li, F. Li, X. Chen, L. Sun, J. Jia, J. Wu, X. Jiang, J. Wang, Y. Huang, Q. Wang, Y. Zhou, L. Deng, T. Xi, L. Ma, T. Hu, Q. Zhang, Y. Chen, N. Liu, X. Wang, Z. Zhu, C. Lu, R. Shu, C. Peng, J. Wang, and J. Pan, Nature **549**, 43 (2017).
13. I. M. Vellekoop and A. P. Mosk, Opt. Lett. **32**, 2309 (2007).
14. M. Nixon, O. Katz, E. Small, Y. Bromberg, A. Friesem, and Y. Davidson, Nat. Photonics **7**, 919 (2013).
15. P. Lai, L. Wang, J. W. Tay, and L. Wang, Nat. Photonics **9**, 126 (2015).
16. R. Horstmeyer, H. Ruan, and C. Yang, Nat. Photonics **9**, 563 (2015).
17. Y. Qiao, X. Chen, Y. Peng, and Y. Zheng, Opt. Lett. **42**, 1895 (2017).
18. J. Aulbach, B. Gjonaj, P. Johnson, and A. Lagendijk, Opt. Express **20**, 29237 (2012).
19. T. Strudley, R. Bruck, B. Mills, and O. L. Muskens, Light Sci. Appl. **3**, e207 (2014).
20. H. Defienne, M. Barbieri, I. A. Walmsley, B. J. Smith, and S. Gigan, Sci. Adv. **2**, e1501054 (2016).
21. J.-L. Blanchet, F. Devaux, L. Furfaro, and E. Lantz, Phys. Rev. Lett. **101**, 233604 (2008).
22. V. Bermudez, F. Caccavale, C. Sada, F. Segato, and E. Dieguez, J. Cryst. Growth **191**, 589 (1998).
23. Y. Furukawa, K. Kitamura, and S. Takekawa, Opt. Lett. **23**, 1892 (1998).
24. M. Mounaix, D. Andreoli, H. Defienne, G. Volpe, O. Katz, S. Grésillon, and S. Gigan, Phys. Rev. Lett. **116**, 253901 (2016).
25. Y. Qiao, Y. Peng, Y. Zheng, F. Ye, and X. Chen, Opt. Lett. **43**, 787 (2018).
26. T. B. Pittman, B. C. Jacobs, and J. D. Franson, Opt. Commun. **246**, 545 (2005).
27. M. D. C. Pereira, F. E. Becerra, B. L. Glebov, J. Fan, S. W. Nam, and A. Migdall, Opt. Lett. **38**, 1609 (2013).
28. D. B. Conkey, A. N. Brown, A. M. Caravaca-Aguirre, and R. Piestun, Opt. Express **20**, 4840 (2012).
29. H. B. de Aguiar and S. Brasselet, Phys. Rev. A **94**, 043830 (2016).
30. I. M. Vellekoop and A. P. Mosk, Opt. Commun. **281**, 3071 (2008).
31. M. J. Collins, C. Xiong, I. H. Rey, T. D. Vo, J. He, S. Shahnia, C. Reardon, T. F. Krauss, M. J. Steel, A. S. Clark, and B. J. Eggleton, Nat. Commun. **4**, 2582 (2013).
32. B. S. Jeon, J. S. Yoo, and J. D. Lee, J. Electrochem. Soc. **143**, 3923 (1996).
33. T. Xiang, Y. Li, Y. Zheng, and X. Chen, Opt. Express **25**, 12493 (2017).